Title
Shear Forces Enhance Toxoplasma gondii Tachyzoite Motility on Vascular Endothelium

Journal
mBio, 5(2)

ISSN
2150-7511

Authors
Harker, K. S
Jivan, E.
McWhorter, F. Y
et al.

Publication Date
2014-04-01

DOI
10.1128/mBio.01111-13

RESEARCH ARTICLE

Shear Forces Enhance *Toxoplasma gondii* Tachyzoite Motility on Vascular Endothelium

Katherine S. Harker,[a,b] Elizabeth Jivan,[a,b] Frances Y. McWhorter,[c,d,e] Wendy F. Liu,[c,d,e] Melissa B. Lodoen[a,b]

Department of Molecular Biology and Biochemistry,[a] Institute for Immunology,[b] Department of Biomedical Engineering,[c] Department of Chemical Engineering and Materials Science,[d] and the Edwards Lifesciences Center for Advanced Cardiovascular Technology,[e] University of California, Irvine, California, USA

ABSTRACT ***Toxoplasma gondii* is a highly successful parasite that infects approximately one-third of the human population and can cause fatal disease in immunocompromised individuals. Systemic parasite dissemination to organs such as the brain and eye is critical to pathogenesis. *T. gondii* can disseminate via the circulation, and both intracellular and extracellular modes of transport have been proposed. However, the processes by which extracellular tachyzoites adhere to and migrate across vascular endothelium under the conditions of rapidly flowing blood remain unknown. We used microfluidics and time-lapse fluorescence microscopy to examine the interactions between extracellular *T. gondii* and primary human endothelial cells under conditions of physiologic shear stress. Remarkably, tachyzoites adhered to and glided on human vascular endothelium under shear stress conditions. Compared to static conditions, shear stress enhanced *T. gondii* helical gliding, resulting in a significantly greater displacement, and increased the percentage of tachyzoites that invaded or migrated across the endothelium. The intensity of the shear forces (from 0.5 to 10 dynes/cm^2) influenced both initial and sustained adhesion to endothelium. By examining tachyzoites deficient in the *T. gondii* adhesion protein MIC2, we found that MIC2 contributed to initial adhesion but was not required for adhesion strengthening. These data suggest that under fluidic conditions, *T. gondii* adhesion to endothelium may be mediated by a multistep cascade of interactions that is governed by unique combinations of adhesion molecules. This work provides novel information about tachyzoite interactions with vascular endothelium and contributes to our understanding of *T. gondii* dissemination in the infected host.**

IMPORTANCE ***Toxoplasma gondii* is a global parasite pathogen that can cause fatal disease in immunocompromised individuals. An unresolved question is how the parasites circulate in the body to tissues to cause disease. *T. gondii* parasites are found in the bloodstream of infected animals and patients, and they have been shown to adhere to and cross the endothelial cells that line blood vessel walls. To investigate these interactions, we devised a microfluidic system to visualize parasites interacting with vascular endothelium under conditions similar to those found in the bloodstream. Interestingly, parasite migration was significantly influenced by the mechanical force of shear flow. Furthermore, we identified a role for the parasite surface protein MIC2 in the initial phase of adhesion. Our study is the first to document *T. gondii* interactions with endothelium under shear stress conditions and provides a foundation for future studies on the molecules that mediate parasite interaction with the vasculature.**

Received 20 December 2013 **Accepted** 10 March 2014 **Published** 1 April 2014

Citation Harker KS, Jivan E, McWhorter FY, Liu WF, Lodoen MB. 2014. Shear forces enhance *Toxoplasma gondii* tachyzoite motility on vascular endothelium. mBio 5(2):e01111-13. doi:10.1128/mBio.01111-13.

Editor Louis Weiss, Albert Einstein College of Medicine

Address correspondence to Melissa B. Lodoen, mlodoen@uci.edu.

Toxoplasma gondii is a single-celled eukaryotic parasite that is found worldwide (1). Infection predominantly occurs through the ingestion of parasite tissue cysts or oocysts from contaminated food or water (2). In immunocompetent individuals, a robust cellular and humoral immune response controls the infection, and the parasite establishes a latent state. In immunosuppressed individuals, however, infection can result in severe toxoplasmosis, due either to reactivation of encysted parasites or to acute infection (1).

The spread of *T. gondii* from the intestine into secondary tissues is critical for pathogenesis (3). Infection results in colonization of the heart, brain, eye, skeletal muscle, and kidney (2, 4). Many recent studies on *T. gondii* dissemination have focused on an intracellular mode of transport in motile leukocytes (5–9). However, free *T. gondii* parasites are found in the blood of acutely infected mice (5) and humans (10), and *in vitro* assays have shown that extracellular tachyzoites can adhere to and cross polarized epithelial cell barriers (11) and retinal endothelium (12), suggesting that an extracellular mode of dissemination may also be employed, depending on the tissue or site in the body.

T. gondii uses an actomyosin motor complex to power substrate-dependent gliding motility and invasion (13). The parasite secretes adhesion proteins from apical secretory organelles called the micronemes. These adhesins are anchored to the parasite surface via their cytoplasmic domains, which associate with the parasite actin cytoskeleton via an aldolase bridge (14). The adhesins "treadmill" along the length of the parasite, propelling it forward, and are cleaved at the posterior end. *T. gondii* gliding

motility has been largely studied *in vitro* by the examination of adhesion trails (15, 16) or by live-cell microscopy (17, 18) on protein-coated glass. Håkansson et al. defined three major types of parasite motility: circular and helical gliding, which produce net forward movement, and twirling, which does not (17). Similar modes of movement have also been described for other members of the phylum Apicomplexa, including *Plasmodium* (19) and *Cryptosporidium* sporozoites (20).

T. gondii dissemination in the body occurs via the circulation. To leave the bloodstream and enter tissues, the parasites must adhere to vascular endothelial cells and cross the endothelial barrier under conditions of blood flow. Whether *T. gondii* parasites are capable of completing this processes as extracellular tachyzoites has not been examined. Using a system combining live-cell microscopy with microfluidics, we performed an in-depth analysis of parasite adhesion and motility under conditions of physiologic shear stress. Remarkably, *T. gondii* tachyzoites adhere and glide on human endothelium under flow conditions. Fluidic shear stress significantly influenced motility dynamics and the outcome of parasite interactions with endothelium. Lastly, we identified a distinct role for the parasite microneme protein 2 (MIC2) in the initial adhesion events of *T. gondii* to endothelium under conditions of shear flow.

RESULTS

Extracellular *T. gondii* tachyzoites adhere to endothelium and are motile under shear stress conditions. To examine *T. gondii* tachyzoites under conditions of fluidic shear stress, we modified our previously described fluidic system (8) to a microfluidic scale. We characterized parasite interactions with primary human umbilical vein endothelial cells (HUVEC) and with fetal bovine serum (FBS)-coated glass, which is commonly used to examine *T. gondii* motility (17, 21, 22). Following syringe lysis, *T. gondii* tachyzoites were added to wells of a chamber slide (static condition) or perfused into a microfluidic channel (flow condition) at 0.5 dyne/cm^2, and movements were tracked at the apical end of the parasite for the 30 s after contact with either HUVEC or FBS. Interestingly, extracellular *T. gondii* were capable of adhesion and motility under shear stress conditions on both HUVEC and FBS (see Videos S1 and S2, respectively, in the supplemental material). Under both static and shear stress conditions, parasites that adhered to FBS moved at higher velocities than those that adhered to HUVEC. In addition, parasites that adhered to FBS traveled greater distances from where they initiated adhesion than those that adhered to HUVEC (Fig. 1; also, see Fig. S1 in the supplemental material). The total pathlength is the total distance a parasite travels, whereas the maximum displacement is the greatest distance a parasite travels from the point where it initially adheres. Interestingly, the introduction of shear flow significantly increased the maximum displacement of tachyzoites on both substrates, without affecting their total pathlength (Fig. 1B).

We next wanted to determine if shear force influenced the likelihood of parasites remaining attached to the endothelial surface or of invasion or migration across the endothelial barrier. To address this, we observed tachyzoites interacting with endothelium under flow conditions for 12 min and categorized their location every 30 s after their adhesion to the monolayer. We found that parasites remained attached to the endothelial surface, moved into or below the endothelium (identified as dim by differential interference contrast [DIC] illumination), or detached from the monolayer (Fig. 2A). Tachyzoite movement in the *z* direction was most dynamic immediately after adhesion: most of the parasites that entered the monolayer did so within 4 min, and beyond this time point, there were very few changes in parasite location in the *z* direction. To determine whether the addition of shear force influenced parasite invasion or migration across the monolayer, we compared parasite location under static and flow conditions within this dynamic period. Under static conditions, 85% of the parasites remained on the surface of the HUVEC at 3 min post-adhesion, whereas 15% had entered the endothelium (Fig. 2B). Notably, we observed a nearly 2.5-fold increase in the percentage of parasites that migrated into or below the HUVEC monolayer under conditions of shear stress (Fig. 2B). Collectively, these data suggest that shear forces significantly affect parasite movement and the outcome of tachyzoite interactions with endothelium.

Characterization of *T. gondii* motility on HUVEC under shear stress conditions. To qualitatively and quantitatively examine parasite migration under flow conditions, a detailed analysis of motility was performed. Under conditions of shear stress, parasites performed all three types of *T. gondii* movement (17): helical gliding, circular gliding, and twirling. Tachyzoites also moved "nonproductively," i.e., they exhibited movement characterized by stretching and retracting along the longitudinal axis and oscillation, which did not produce net forward movement along the plane of the substrate. Motionless tachyzoites were also observed and were characterized as stationary. Time-lapse images and videos of representative parasites performing helical gliding, circular gliding, or twirling on endothelium under shear stress conditions were acquired (Fig. 3; also, see Videos S3 to S5 in the supplemental material). The path and velocity of each parasite, as determined by tracking at the apical end, are shown. Tracking was done at the apical end because this allowed clear resolution of the transitions between the different modes of parasite motility. Moreover, apical-end tracking allowed us to gain information about parasite movements that did not necessarily result in net forward motion. For instance, tracking twirling parasites at the apical end permitted an analysis of twirling "velocity," which varied for individual parasites. During helical gliding (Fig. 3A; also, see Video S3 in the supplemental material), a characteristic 180° rotation around the longitudinal axis occurred between 31 and 34 s, producing a spike in instantaneous velocity (Fig. 3A), as has been previously reported (17). Two additional helical turns occurred between 43 and 46 s and between 49 and 52 s. After each turn, the parasite reoriented, moving at velocities of up to 2 μm/s. During circular gliding, the clockwise circular motion of the parasite was evident in the shape of the trace produced from tracking analysis (Fig. 3B). In contrast to helical gliding, circular gliding occurred at relatively low velocities (typically less than 4 μm/s) and was characterized by momentary pauses (see Video S4 in the supplemental material). During twirling, the parasites were oriented vertically, with the posterior end anchored to the substrate, and a tilting rotation was observed (Fig. 3C; also, see Video S5 in the supplemental material). On average, the apical end of parasites under shear stress conditions twirled at relatively low velocity (2 to 4 μm/s) with sporadic peaks in instantaneous velocity, indicative of a reorientation event similar to that of helical gliding, but without net forward movement parallel to the endothelial monolayer. A minority of the population was also observed performing higher-velocity twirling (>7 μm/s).

We frequently observed tachyzoites exhibiting multiple types

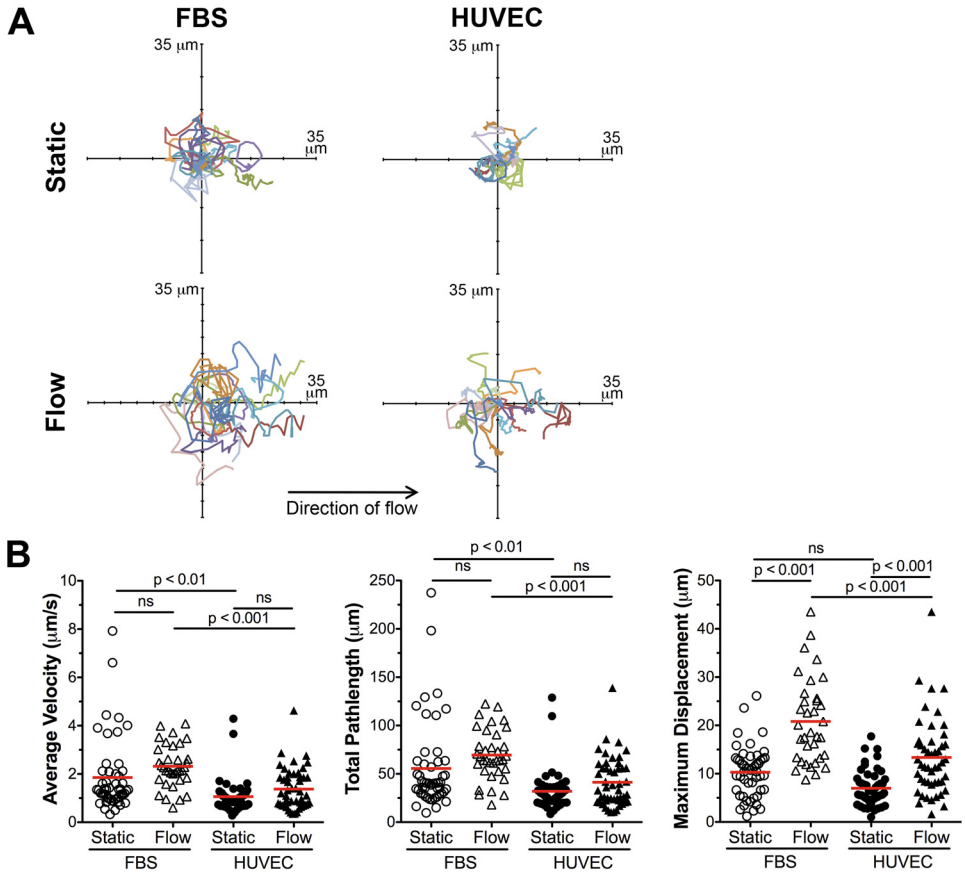

FIG 1 Extracellular *T. gondii* tachyzoites adhere to and are motile on HUVEC under static and shear stress conditions. *T. gondii* tachyzoites were added to FBS-coated glass or confluent monolayers of HUVEC in either a chamber slide (static conditions) or in the microfluidic channel (flow conditions). (A) Representative cell traces of extracellular tachyzoites on FBS or HUVEC under static or flow conditions are shown. Each trace begins at the origin and shows the path of a single parasite ($n = 15$ for all conditions). The direction of flow is from left to right. (B) The average velocity, total pathlength traveled, and maximum displacement reached by each parasite during the first 30 s post-adhesion are shown. Each data point represents a single parasite. Three independent experiments were performed, and the data were pooled ($n_{\text{FBS, Static}} = 50$; $n_{\text{FBS, Flow}} = 35$; $n_{\text{HUVEC, Static}} = 50$; $n_{\text{HUVEC, Flow}} = 49$). The red bar indicates the mean for the group. ANOVA with a Tukey comparison of all means was used to compare multiple means.

of motility over time (Fig. 4A and B; also, see Video S6 in the supplemental material). To better understand these complex parasite movements and the effects of substrate and fluidic shear stress, parasite motility was classified at either 10 s or 60 s after adhesion to either FBS or HUVEC and under static or flow conditions (Fig. 4C and D). The percentages of parasites that were moving, nonproductive, or stationary under each condition are shown (Fig. 4C). For parasites that moved productively in Fig. 4C, the absolute numbers of parasites performing helical or circular gliding or twirling were graphed (Fig. 4D). For parasites on FBS, the percentage of the parasite population that was motile remained relatively constant over time (Fig. 4C), but the addition of shear stress resulted in a significantly larger portion of parasites performing helical gliding (Fig. 4D). In contrast, for parasites that adhered to HUVEC, shear stress conditions increased the proportion of motile parasites immediately following adhesion (10 s) and specifically enhanced helical and circular gliding; however, these highly dynamic modes of motility declined over time (60 s). When we examined the motility of a representative subset of 15 parasites during their entire first minute post-adhesion, we observed similar trends (Fig. 5). We also observed a fraction of parasites that reinitiated motility after prolonged stationary periods. These data indicate that flow conditions increased dynamic, productive motility (helical and circular gliding) immediately after attachment, which may contribute to the increased displacement observed for parasites under shear stress (Fig. 1).

Initial and sustained parasite adhesion at increasing shear force. The initial adhesion and in-depth motility analyses of extracellular tachyzoites were performed at 0.5 dyne/cm^2, a relatively low physiological shear stress (23). To address the effects of higher levels of shear stress on parasite adhesion, *T. gondii* tachyzoites were flowed over confluent monolayers of HUVEC at 0.5, 2, 5, or 10 dynes/cm^2 for 3 min, and adhesion events were counted. An adhesion event was defined as a parasite that appeared on the endothelial surface and remained attached in the plane of focus for a minimum of 4 s. As shear force increased, we observed a decrease in the number of adhesion events (Fig. 6A; also, see Fig. S2 in the supplemental material).

We next investigated the adhesion strength of tachyzoites by examining their response to an increase in shear stress. This can be addressed by allowing adhesion to occur under static or low-shear conditions and then increasing the flow rate (24). To do this, tachyzoites were flowed over HUVEC at 0.5 dyne/cm^2 for 3 min to allow for adhesion, and then the shear stress was maintained at

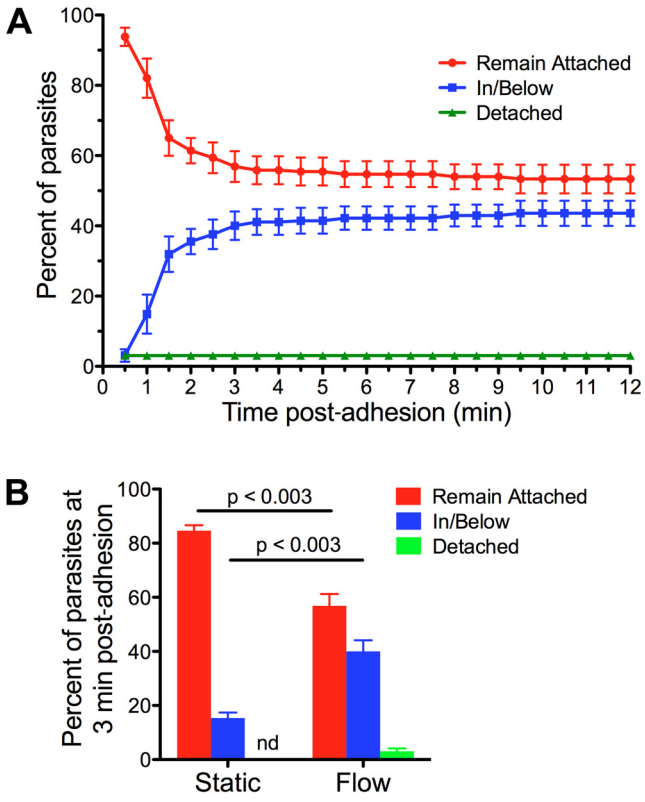

FIG 2 Influence of shear stress on *T. gondii* movement into and/or across the endothelium over time. (A) *T. gondii* tachyzoites were flowed over HUVEC in the microfluidic channel for 12 min, and their interactions with the endothelium were analyzed. Parasites were considered adherent when they were in contact with the endothelial surface for a minimum of 4 s. The location of each adherent parasite was assessed at 30-s intervals post-adhesion. The percentages of parasites that remained attached to (red circles), moved in/below (blue squares), or detached from (green triangles) the HUVEC are shown. Three independent experiments were performed, and the data were pooled (n = 211). Bars represent means ± standard errors of the means (SEM). (B) *T. gondii* tachyzoites were added to HUVEC in either a chamber slide (static conditions) or in the microfluidic channel (flow conditions). At 3 min post-adhesion, the percentages of parasites that remained attached to (red), moved in/below (blue), or, in the flow condition, detached from (green) the HUVEC are shown (n_{Static} = 431; n_{Flow} = 211). For each condition, at least two independent experiments were performed, and the data were pooled. Bars represent means and SEM. nd, no data. Student's two-tailed t test with Welch's correction was used for pairwise comparisons.

0.5 dyne/cm^2 or increased to 2, 5, or 10 dynes/cm^2 for an additional 3 min. Parasites could adhere at any point during the first 3 min of flow; however, only those that were attached to the HUVEC surface at the switch in shear force were analyzed. The percentage of adherent tachyzoites that remained attached, entered the monolayer (in/below), or detached after the switch in shear stress was determined. We found that the percentage of adherent parasites that detached from the monolayer increased as shear stress increased (Fig. 6B). The increase in shear stress, however, did not affect the proportion of parasites that entered the monolayer ("in/below" category in Fig. 6B). These data indicate that the intensity of the shear stress influences the number of parasites that adhere to the endothelium and their ability to sustain adhesion; however, it does not appear to affect their likelihood of moving into or below the monolayer, at least at shear forces up to 10 dynes/cm^2.

Invasion or transmigration of *T. gondii* under shear stress conditions. We reasoned that parasites migrating into or below the monolayer may be invading the endothelium, as has been previously reported (25), or transmigrating across the endothelial barrier via a paracellular or transcellular route. We also wanted to determine if shear force influenced these possible outcomes of movement into the monolayer. For the static condition, tachyzoites were incubated on HUVEC monolayers for 20 min and then washed and fixed. For shear stress conditions, *T. gondii* were flowed over the endothelium for 1 to 2 min, and a Y-valve connector was used to flow medium alone without disrupting flow for a total of 20 min. Fluidic channels were then perfused with fixative. Under both conditions the cells were then stained with antibodies against the parasite dense granule protein GRA7, as a marker for invasion. In extracellular tachyzoites, GRA7 is found in the dense granules, whereas in infected host cells, GRA7 localizes to the parasitophorous vacuole (PV) (26). In both static and flow conditions, we observed tachyzoites that appeared dim by DIC illumination (in/below) and were either surrounded by GRA7 staining or not (Fig. 7A). Under static conditions, 81% of DIC-dim parasites localized to GRA7$^+$ vacuoles, whereas 19% were not associated with GRA7 staining. Interestingly, flow conditions significantly increased the percentage of DIC-dim parasites that were GRA7$^-$ (35% of the population) (Fig. 7B). The DIC-dim GRA7$^-$ population likely included parasites that had completed transmigration and were under the monolayer. Indeed, in live-cell imaging experiments, we have observed tachyzoites that continued to migrate under the endothelium after entering the monolayer. We cannot exclude the possibility that some of the DIC-dim GRA7$^-$ tachyzoites were in the process of transcytosis at the time of analysis (in a vesicle that lacked GRA7) or had invaded immediately prior to fixation and had yet to secrete a sufficient amount of GRA7 into the PV to be detectable by immunofluorescence assay (IFA). Collectively, these data indicate that the majority of tachyzoites that enter the endothelium under shear stress and static conditions invade the monolayer and form a PV, and that flow conditions may result in a greater percentage of parasites that breach the barrier and undergo transmigration.

Role of MIC2 in adhesion to HUVEC under shear stress conditions. We next sought to address the role of parasite adhesion proteins in interactions with the endothelium under shear stress conditions and the possibility that different parasite adhesins may contribute to distinct stages of the *T. gondii* adhesion cascade in shear stress. One of the best-characterized *T. gondii* surface proteins associated with adhesion and motility is the microneme protein MIC2 (21, 27–30). Under static assay conditions, MIC2 was found to be important for attachment to host cells, helical gliding, and invasion (21). However, a role for MIC2 in adhesion to vascular endothelium or under conditions of shear stress has not yet been examined. To address this possibility, we employed a conditional MIC2 knockdown system developed and generously provided by the Carruthers lab (21). Parental tTA-dhfr parasites and the Δ*mic2e*/*mic2i* conditional MIC2 knockdown parasite line, which uses a tetracycline-responsive promoter to control the expression of MIC2, were used. The addition of anhydrotetracycline (ATc) reduced the expression of MIC2 as determined by both immunofluorescence assay (Fig. 8A) and Western blotting (Fig. 8B). The tTA-dhfr and ATc-treated Δ*mic2e*/*mic2i* tachyzoites were labeled with different fluorescent dyes, mixed 1:1, and perfused over a HUVEC monolayer, and adhesion events

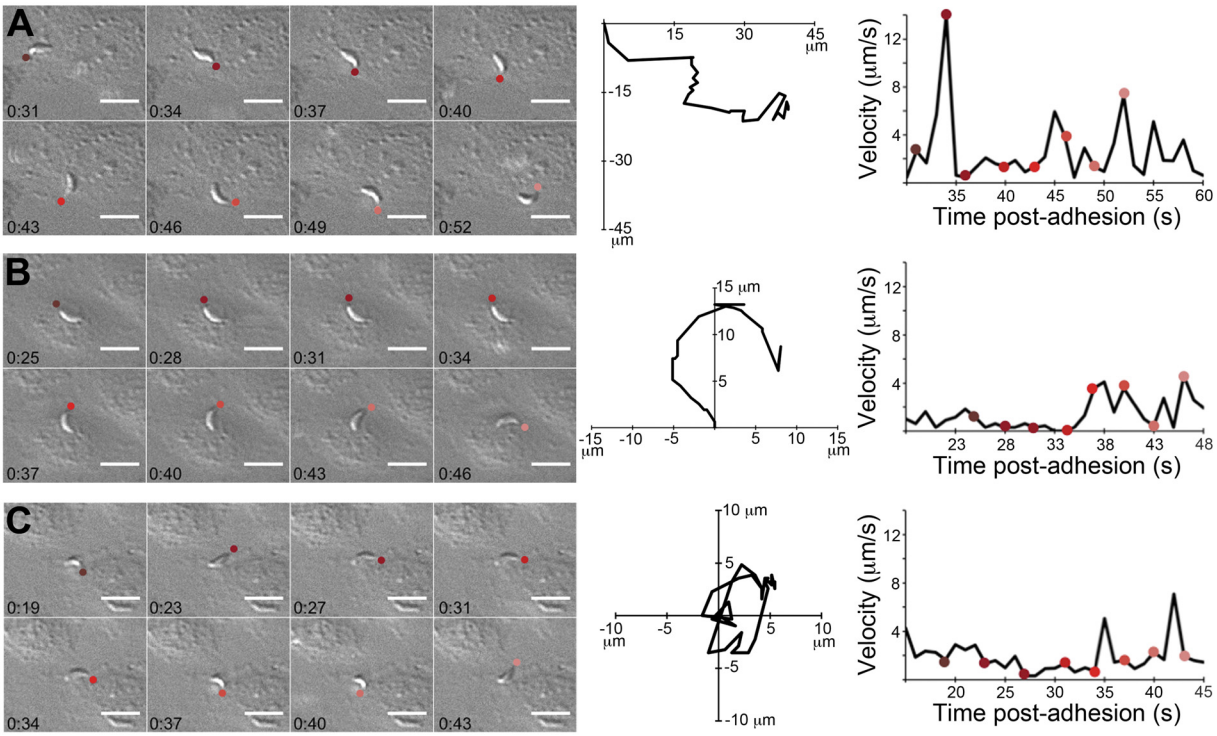

FIG 3 Modes of *T. gondii* motility on HUVEC under shear stress conditions. *T. gondii* tachyzoites were flowed over HUVEC at 0.5 dyne/cm^2. Cell tracking software was used to track the movements at the apical end of the parasite (designated with a colored circle). Representative time-lapse images of parasites performing helical gliding (A), circular gliding (B), or twirling (C) are shown. The path of the apical end of the parasite and the instantaneous velocity at the apical end are shown for each mode of motility. The colored dots in the velocity-versus-time plots correspond to those in the time-lapse images. The direction of flow is from left to right. Bars, 10 μm.

under flow conditions were counted along the entire length of the fluidic channel. A sample of the mixture was used to determine the precise input ratio of the two strains by both flow cytometry and by microscopy (data not shown). The ratio of tTA-dhfr and ATc-treated Δ*mic2e*/*mic2i* tachyzoite adhesion events in the channel relative to the input ratio was calculated. A value of 1 indicates equivalent adhesion of the two populations. We observed a consistent underrepresentation of the ATc-treated Δ*mic2e*/*mic2i* parasites compared to the tTA-dhfr parasites (Fig. 8C). To control for the possibility that treatment with ATc affected adhesion, we evaluated the adhesion of ATc-treated and untreated tTA-dhfr parasites under static conditions and found no significant difference in their adhesion (see Fig. S3A in the supplemental material). In addition, when we examined adhesion in a static assay, we observed a similar underrepresentation of ATc-treated Δ*mic2e*/*mic2i* parasites compared to the tTA-dhfr parasites (see Fig. S3B). These data indicate that MIC2 contributes to *T. gondii* adhesion to endothelium in shear stress; however, a portion of ATc-treated Δ*mic2e*/*mic2i* parasites were still capable of adhesion under these conditions. Although we observed that MIC2 levels were substantially reduced in ATc-treated parasites, it is possible that a low level of MIC2 expression in these treated parasites contributed to this residual adhesion.

We next investigated a potential role for MIC2 in adhesion strengthening under conditions of increasing shear stress. To do this, a mixture of tTA-dhfr and ATc-treated Δ*mic2e*/*mic2i* tachyzoites were perfused over a HUVEC monolayer at 0.5 dyne/cm^2 to allow adhesion to occur. The shear stress was then increased to 10 dynes/cm^2. The percentage of tachyzoites that remained attached or that detached from the monolayer after the increase in shear force was calculated. Interestingly, the tTA-dhfr and ATc-treated Δ*mic2e*/*mic2i* tachyzoites remained similarly attached to the endothelium after the increase in shear stress to 10 dynes/cm^2 (Fig. 8D): for both populations of parasites, approximately 50% of the tachyzoites detached after the transition to increased shear force. Collectively, these data suggest that MIC2 plays an important role in the initial phase of attachment to the endothelium but is not required for adhesion strengthening and that other parasite adhesins may mediate these sustained interactions with the endothelium.

DISCUSSION

Dissemination of *T. gondii* from the primary site of infection to secondary tissues is thought to occur through both intracellular and extracellular mechanisms (3). To leave the bloodstream, tachyzoites interacting with blood vessel walls must contend with the mechanical forces of shear stress. Live-cell microfluidic systems provide a highly tunable method for characterizing cellular adhesion and motility and analyzing the role of specific adhesins in attachment to human cellular substrates under flow conditions. Our current study shows that tachyzoites can adhere to and migrate on vascular endothelium under conditions of physiologic shear stress. In addition, we found that shear forces enhance dynamic motility and the likelihood of invasion and/or transmigration, both of which are critical components of pathogenesis. These findings support the relevance of including mechanical force as an

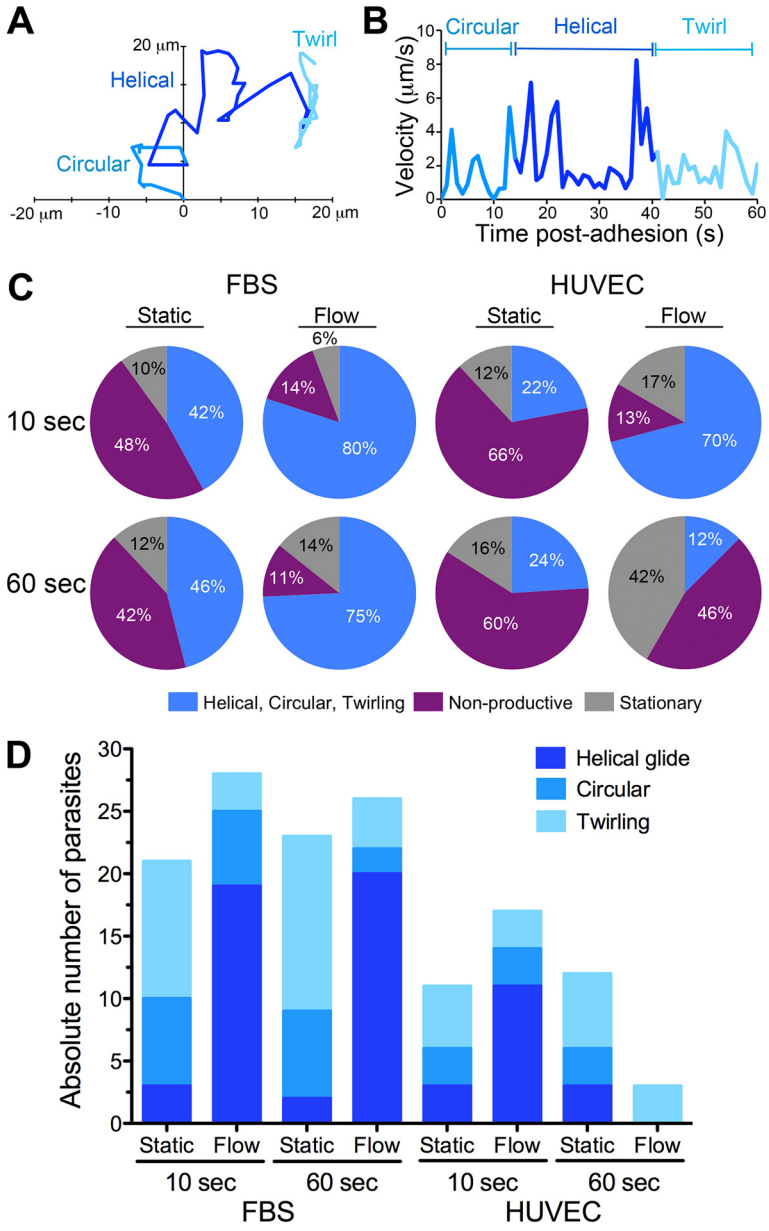

FIG 4 Characterization of parasite motility under static and shear stress conditions. *T. gondii* tachyzoites were added to FBS or HUVEC in either a chamber slide (static conditions) or the microfluidic channel (flow conditions). (A) The trace generated by a tachyzoite exhibiting three modes of motility within 1 min post-adhesion to HUVEC under flow conditions is shown. (B) A velocity plot over time is shown for the parasite examined in panel A. (C) The percentages of motile, nonproductive, and stationary parasites at either 10 s or 60 s after adhesion to FBS or HUVEC under static or flow conditions are shown ($n_{\text{FBS, Static}} = 50$; $n_{\text{FBS, Flow}} = 35$; $n_{\text{HUVEC, Static}} = 50$; $n_{\text{HUVEC, Flow}} = 49$). (D) The absolute numbers of motile parasites (from panel C) undergoing helical or circular gliding or twirling at either 10 s or 60 s after adhesion to FBS or HUVEC under static or flow conditions are shown. $n_{\text{FBS, Static, 10 s}} = 21$; $n_{\text{FBS, Flow, 10 s}} = 28$; $n_{\text{FBS, Static, 60 s}} = 23$; $n_{\text{FBS, Flow, 60 s}} = 26$; $n_{\text{HUVEC, Static, 10 s}} = 11$; $n_{\text{HUVEC, Flow, 10 s}} = 17$; $n_{\text{HUVEC, Static, 60 s}} = 12$; $n_{\text{HUVEC, Flow, 60 s}} = 3$.

additional experimental parameter in understanding patterns of parasite migration. In addition, recent work on *T. gondii* motility in a three-dimensional system revealed that tachyzoites move through Matrigel in a corkscrew-like trajectory distinct from that observed in two-dimensional assays (31), further reinforcing the value of incorporating conditions that more closely mimic *in vivo* environments.

Multistep adhesion cascades are used by both circulating mammalian cells (32) and pathogens (33, 34) to exit the bloodstream. However, the precise manner in which these interactions occur appears to vary. Initial adhesion interactions, often referred to as "tethering" or "capture," are transient, occur at high velocities, and serve to decelerate the adhering cell. In *Borrelia burgdorferi*, tethering is mediated by the fibronectin-binding domain of the bacterial adhesin BBK32 and is the essential first interaction that decelerates the bacterium and brings it into close contact with the endothelial cell surface (34). For *Plasmodium berghei*, initial sporozoite adhesion to glass flow chambers requires the

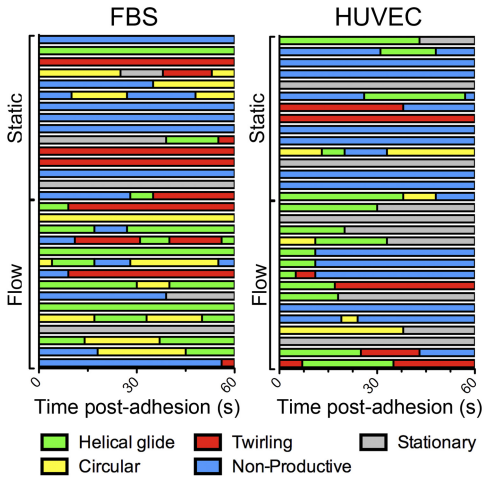

FIG 5 Parasite motility over time under static and shear stress conditions. *T. gondii* tachyzoites were added to FBS or HUVEC in either a chamber slide (static conditions) or the microfluidic channel (flow conditions). The motility of a representative subset of 15 parasites under each condition over time is shown, with each bar representing the motility of a single parasite.

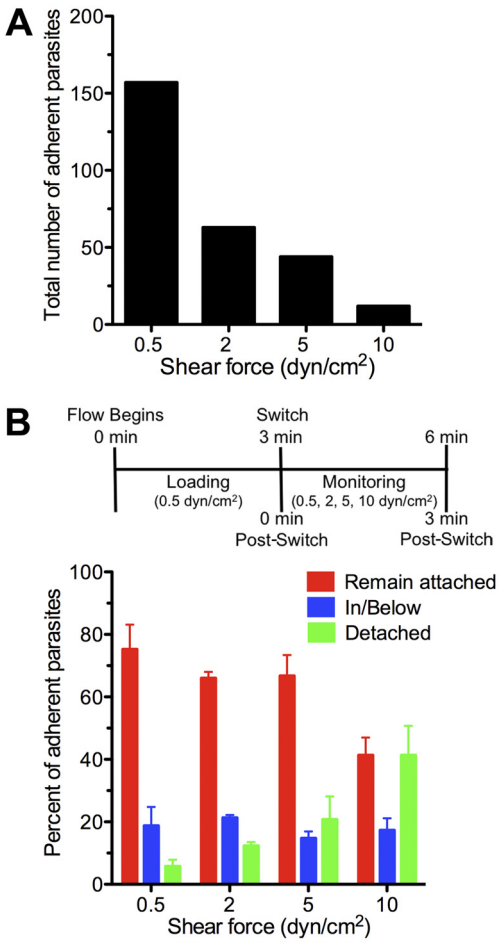

FIG 6 Initial and sustained adhesion with increasing shear force. *T. gondii* tachyzoites were flowed over confluent monolayers of HUVEC in the microfluidic channel. (A) The total numbers of parasite adhesion events at shear forces of 0.5, 2, 5, and 10 dynes/cm² are shown. The graph represents aggregated data from 4 independent microfluidic experiments ($n = 468$). (B) *T. gondii* tachyzoites were flowed over HUVEC at 0.5 dyne/cm² for a 3 min "loading" phase. The shear force was then maintained at 0.5 dyne/cm² or switched to 2, 5, or 10 dynes/cm². Parasites that were attached to the endothelial surface at the time of the switch were monitored for an additional 3 min. The percentage of adherent parasites that remained attached to, moved inside/below, or detached from the HUVEC monolayer during the "monitoring" phase is shown. Bars represent means and SEM. $n = 276$ from 4 independent experiments.

parasite adhesins TRAP and S6 (33). Following initial adhesion, transient adhesion associated with a phase of rolling or active motility occurs. *P. berghei* sporozoites wave or glide (33), whereas *B. burgdorferi* organisms perform dragging mediated by the glycosaminoglycan-binding domain of BBK32 (34). Subsequently, a transition to firm adhesion occurs. For *B. burgdorferi* a period of "stationary adhesion" near endothelial cell junctions immediately follows dragging and precedes transmigration and escape from the vasculature (35). A similar period of sustained firm adhesion prior to extravasation has been documented for *P. berghei* exiting blood vessels in the mouse dermis (36). We frequently observed that *T. gondii* gliding on endothelium was punctuated by periods of motionless activity, sometimes lasting several minutes, prior to reinitiation of migration. One potential explanation for these patterns is fluctuation in intracellular cation concentration. Intraparasitic calcium mobilization has been shown to coordinate microneme secretion (37) and influence motility (38). In addition, parasite egress is regulated by both potassium and calcium flux (39).

Our data suggest that *T. gondii* tachyzoite adhesion to endothelium under shear stress conditions could also be divided into a multistep cascade. It is likely that a combination of adhesion molecules, potentially with overlapping functions, mediate *T. gondii* adhesion under shear stress conditions. In our studies, MIC2 clearly played a role in this process. However, under conditions of increasing shear stress the MIC2-deficient parasites remained as adherent as the parental control parasites, implying a role for MIC2 in initial parasite adhesion that may be distinct from adhesion strengthening. One potential ligand for MIC2 on the endothelium is ICAM-1. MIC2 has been shown to interact with ICAM-1 to mediate *T. gondii* transepithelial migration (30), and ICAM-1-dependent transmigration across retinal endothelium has been observed (12). In our assays, a portion of the MIC2-deficient parasites were capable of adhesion to endothelium under shear stress conditions, indicating that other parasite factors may contribute to this process. *T. gondii* has been shown to use a broad range of sulfated glycosaminoglycans to bind to substratum and host cells in static systems (40). Other microneme proteins are also known to contribute to parasite adhesion, invasion, and virulence in mice (41). MIC1 binds host glycans, and a conserved microneme adhesive repeat (MAR) recognizes sialic acid and contributes to invasion (42, 43). The chitin binding-like domain of MIC3 is required for attachment to host cells (44, 45). Single gene disruptions of either MIC1 or MIC3 produce mild virulence defects; however, double knockouts produce a severe virulence defect *in vivo* (45). Also, *T. gondii* surface antigen 3 (SAG3) can mediate the recognition of cell surface proteoglycans, such as heparin (46), and SAG3-deficient parasites have a 50 to 60% adhesion deficit in *in vitro* assays and an 80% reduction in virulence *in vivo* (47). Whether carbohydrate-mediated adhesion interactions contribute to tachyzoite capture, motility, sustained adhesion, or

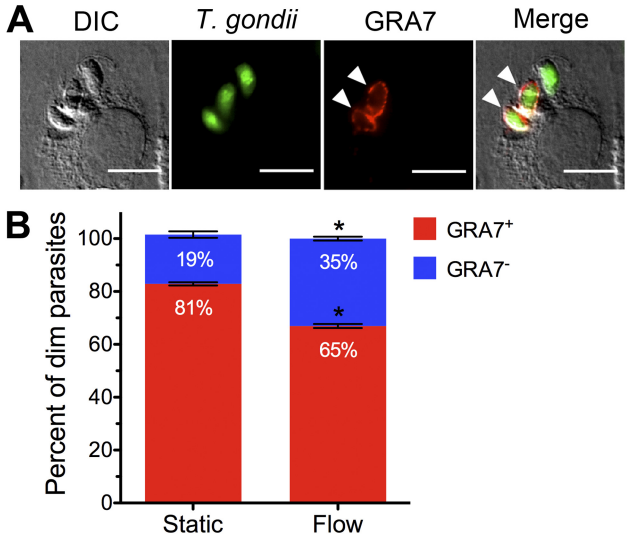

FIG 7 Invasion or transmigration of *T. gondii* under static and shear stress conditions. *T. gondii* tachyzoites were incubated for 20 min with a HUVEC monolayer under either static or shear stress conditions. Coverslips or fluidic channels were then fixed and stained with antibodies against GRA7. (A) Sample micrographs depict DIC-dim parasites (previously categorized as in/below in Fig. 2 and 6B) that are either GRA7$^+$ (white arrowheads) or GRA7$^-$. Bar, 10 μm. (B) The percentages of DIC-dim parasites associated with GRA7 are shown. For each condition, two independent experiments were performed and the data were pooled ($n_{Static} = 499$; $n_{Flow} = 309$). Bars represent means ± SEM. Student's two-tailed *t* test with Welch's correction was used for pairwise comparisons. *, $P < 0.01$ for comparisons between the static and flow conditions.

transmigration under shear stress conditions remains to be investigated.

Interestingly, *T. gondii* migrated farther and at higher velocities on FBS than on endothelial cells, suggesting that the endothelium itself may be a barrier to motility. This may be due to the varied topography of the endothelium and to the adhesion molecules expressed on the endothelial surface. In addition, vascular endothelium is heterogeneous in both structure and function (48), suggesting that the processes by which tachyzoites adhere to distinct endothelial cell types may also differ. Endothelial permeability is also highly modulated by acute and chronic inflammation. *T. gondii* infection induces an inflammatory response characterized by the expression of interleukin 12 (IL-12), tumor necrosis factor alpha (TNF-α), and IL-6 (49). *T. gondii* infection of brain endothelial cells upregulates the expression of ICAM-1 (50), and infection of human retinal epithelial cells upregulates ICAM-1 and the inflammatory cytokines IL-1 and IL-6 (51). The stimulation of endothelial cells with proinflammatory mediators induces a proadhesive phenotype termed "endothelial cell activation" (52, 53). "Activated" endothelium expresses elevated levels of adhesion molecules and has decreased tight-junction integrity, resulting in an increase in barrier permeability (54). The unique response of endothelium to infection-induced inflammatory mediators in a given tissue may impact the likelihood of parasite invasion of that tissue. Ultimately, understanding how these interactions allow *T. gondii* dissemination out of the circulation will provide novel insight into mechanisms of parasite spread into tissues and the development of disease.

MATERIALS AND METHODS

Mammalian and parasite cell culture. HUVEC were cultured in endothelial growth medium 2 (EGM-2) with EGM-2 SingleQuot supplements and growth factors (Lonza, Allendale, NJ). Green fluorescent protein (GFP)-expressing type I *T. gondii* (RH) tachyzoites were maintained in human foreskin fibroblasts (HFF) in Dulbecco's modified Eagle medium (DMEM) with 10% FBS, 2 mM L-glutamine, 100 U/ml penicillin, and 100 μg/ml streptomycin (D-10%), as previously described (55). Parasites were syringe lysed, washed, and processed in a high-potassium buffer and then immediately transferred into D-10% for experimentation to prevent microneme exhaustion prior to adhesion and motility assays (56). All parasite and human cell cultures were tested monthly for *Mycoplasma* contamination and confirmed to be negative.

Fabrication of fluidic systems. Fluidic channels (height [H], 1.5 mm; width [W], 3 mm; length [L], 20 mm) were fabricated as previously reported (8) with the following modification: polydimethylsiloxane (PDMS) was adhered to cover glass by plasma bonding. New microfluidic channels (H, 0.1 mm; W, 1.5 mm; L, 10 mm) were fabricated using standard soft lithographic techniques (57). Briefly, a photomask containing arrays of a 1.5-mm by 10-mm pattern was generated by high-resolution laser printing on a transparency (CAD/Art Services Inc., Bandon, OR). A 100-μm thick layer of negative SU-8 photoresist (MicroChem Corp., Newton, MA) was deposited onto a silicon wafer and exposed to UV through the photomask to polymerize. Unpolymerized SU-8 was removed to create relief structures of the channels on the master. PDMS was then cast from the master, oxygen-plasma cleaned (Harrick O_2; Harrick Plasma, Ithaca, NY), and permanently bonded to glass slides.

Fluidic experiments. Fluidic channels were coated with 20 μg/ml fibronectin and seeded with HUVEC overnight. Microfluidic channels were either coated with a 1:1 mixture of FBS in phosphate-buffered saline (PBS) for a minimum of 1 h or coated with 20 μg/ml fibronectin and seeded with HUVEC for a minimum of 7 h prior to experimentation. Channels were connected to an open-loop flow system as previously described (8), with the flow rate controlled by an 11 Plus dual syringe pump (Harvard Apparatus, Holliston, MA). The device was mounted inside a UNO environmental chamber on the microscope stage (OkoLab, Ottaviano, NA, Italy) and maintained at 37°C and 5% CO_2. Tachyzoites were loaded into the syringe pump and perfused through the channels, and live time-lapse imaging was started immediately after flow was initiated. Imaging was performed on a Nikon Eclipse Ti inverted fluorescence microscope using NIS Elements acquisition software. Fluidic assays were performed at a shear force of 0.5 dyne/cm^2 unless otherwise noted.

Static experiments. Wells of an 8-well chamber slide were either coated with a 1:1 mixture of FBS in PBS for a minimum of 1 h or coated with 20 μg/ml fibronectin and seeded with HUVEC. The chamber slide was maintained at 37°C and 5% CO_2 in a UNO environmental chamber (9), and the wells were inoculated with tachyzoites. Time-lapse DIC imaging was initiated immediately after the addition of parasites. For the MIC2 adhesion assays in static conditions, the parasites were allowed to adhere to HUVEC for 15 min at 37°C, and the cells were washed 3 times with PBS to remove any unadherent parasites. Monolayers were then fixed with 4% paraformaldehyde (PFA; Electron Microscopy Sciences, Hatfield, PA) for 20 min at room temperature. DIC and fluorescence images were acquired in 6 random fields of view per well using a 20× objective.

Parasite tracking. The tracking module of the Nikon NIS Elements AR 3.22.11 software was used to manually track the movements of the apical end of individual tachyzoites. For assays in shear stress, every parasite that entered the field of view was tracked. For static assays, at least the same number of parasites that were tracked under flow conditions were chosen at random and tracked as they came into focus. For plotting the traces of individual parasites, the origin (0.0) was set to the parasite's apical end when it first came into contact with the endothelium. The *x* and *y* coordinates of the apical end in the following frames were then used to plot each parasite's path on the endothelium. The average velocity, total pathlength, and maximum displacement of individual parasites during

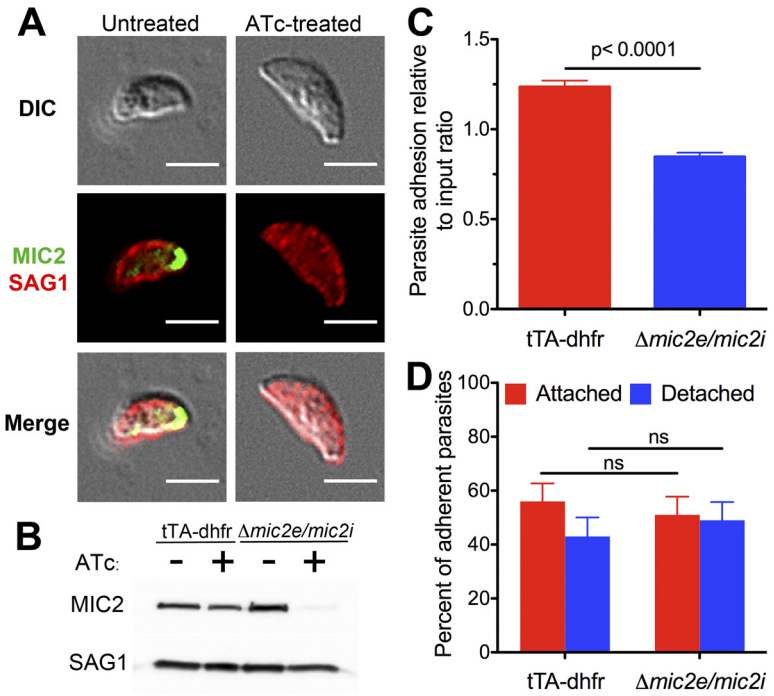

FIG 8 Role of MIC2 in adhesion to HUVEC under shear stress conditions. (A) The Δ*mic2e*/*mic2i* parasites were treated with ATc for 2 days. Extracellular tachyzoites were stained with antibodies against MIC2 or SAG1 and imaged by DIC and by fluorescence for MIC2 expression. Bar, 5 μm. (B) tTA-dhfr and Δ*mic2e*/*mic2i* parasites were untreated or treated with ATc for 2 days. Western blotting was performed to detect MIC2 or SAG1 in the parasite lysates. (C) tTA-dhfr tachyzoites were mixed 1:1 with ATc-treated Δ*mic2e*/*mic2i* tachyzoites and flowed over HUVEC. The parasites were allowed to adhere for 3 min, and DIC and fluorescence images were captured along the entire length of the channel while the cells were still under flow. Parasite adhesion relative to the input ratio is shown. A value of 1.0 would represent equivalent adhesion of the two populations. $n_{\text{tTA-dhfr}} = 1{,}120$; $n_{\text{ATc-treated }\Delta\text{mic2e/mic2i}} = 1{,}073$ (3 independent experiments). (D) A mixture of tTA-dhfr and ATc-treated Δ*mic2e*/*mic2i* parasites were flowed over HUVEC in the microfluidic channel at 0.5 dyne/cm^2 for 3 min, and then the shear stress was increased to 10 dynes/cm^2 for an additional 3 min. The percentage of adherent parasites that remained attached or detached after the increase in shear stress is shown. $n_{\text{tTA-dhfr}} = 70$; $n_{\text{ATc-treated }\Delta\text{mic2e/mic2i}} = 88$ (2 independent experiments). (C and D) Error bars represent means and SEM, and Student's two-tailed *t* test with Welch's correction was used for pairwise comparisons. ns, not significant.

their first 30 s post-adhesion were plotted using Prism (GraphPad Software, La Jolla, CA).

Motility and adhesion assays. To assess parasite adhesion and motility on HUVEC or FBS-coated glass, time-lapse DIC images were acquired using a 20× objective with 1.5× zoom. For the motility assay data shown in Fig. 1, 3, 4, and 5 and in Fig. S1 in the supplemental material, images were acquired every second for up to 10 min, and an adhesion event was defined as the presence of a tachyzoite on the endothelial surface for a minimum of 3 s. Velocity was defined as the distance traveled from one frame to the next divided by the time-lapse. For the sustained adhesion assays in Fig. 2, images were acquired every 4 s for up to 15 min, and an adhesion event was defined as the presence of a tachyzoite on the endothelial surface for a minimum of 4 s. Parasite location in the *z* direction relative to the endothelium was determined by DIC illumination during live-cell imaging. In the initial interactions of tachyzoites with the surface of the endothelium, they appeared bright. Migration into or below the HUVEC monolayer was characterized by the dimming of DIC illumination. By using this change in DIC illumination, the parasites were categorized as remaining attached to, migrating in/below, or detaching from the endothelium. For the adhesion-strengthening assay data shown in Fig. 6 and in Fig. S2 in the supplemental material, perfusion was initiated at 0.5 dyne/cm^2. Three minutes later, the shear stress in the channel was either maintained or increased to 2, 5, or 10 dynes/cm^2. Parasites that adhered during the initial 3 min and remained attached at the surface at the change in shear stress were monitored and categorized as adherent to, detached from, or in/below the endothelium at the conclusion of 6 min of imaging. *De novo* adhesion events that occurred after the switch in shear force were also quantified.

Immunofluorescence microscopy. For GRA7 staining of parasites under static conditions, 5 × 10^5 GFP-expressing RH tachyzoites were added to confluent HUVEC monolayers on coverslips and incubated for 20 min. Coverslips were then washed with PBS and fixed with 4% PFA. The cells were permeabilized and stained for vacuolar GRA7 as previously described (58). Anti-GRA7 antibody (12B6) was a generous gift from P. Bradley (University of California, Los Angeles, CA). For shear stress conditions (Fig. 7), 5 to 10 × 10^6/ml tachyzoites were flowed at 0.5 dyne/cm^2 into fluidic channels over HUVEC. After 1 to 2 min, a Y-valve connector was used to perfuse D-10% through the device, without disrupting flow, for an additional 18 to 20 min. The channels were then perfused with PBS, followed by 4% PFA, and permeabilized and stained as described above. Fluorescence and DIC micrographs were acquired using a 40× or 60× objective.

For the analysis of MIC2 expression, HFF infected with tTA-dhfr or Δ*mic2e*/*mic2i* tachyzoites were cultured in the presence or absence of ATc for 2 days. Tachyzoites were harvested by syringe lysis, added to polylysine-coated coverslips, and fixed with 4% PFA. Samples were stained with anti-MIC2 (6D10) and rabbit anti-SAG1 polyclonal serum (59), followed by Alexa Fluor 305-conjugated goat anti-mouse IgG and Alexa Fluor 594-conjugated goat anti-rabbit IgG (Life Technologies) in PBS containing 3% FBS. Coverslips were mounted with Vectashield (Vector Laboratories, Burlingame, CA). Anti-MIC2 (6D10) was kindly provided by V. Carruthers (University of Michigan, Ann Arbor, MI). To determine the input ratio of fluorescently dyed Δ*mic2e*/*mic2i* and tTA-dhfr parasites, a wet mount of each mixture was analyzed. Images were acquired using a 10× objective with a 1.5× zoom and counted manually.

Western blotting. Parasite cell lysates were separated on 10% SDS-PAGE, transferred to polyvinylidene difluoride (PVDF) membranes, and immunoblotted with mouse anti-MIC2 (6D10) and rabbit anti-SAG1 (59). The membranes were then stained with horseradish peroxidase (HRP)-conjugated anti-mouse and anti-rabbit IgG (Jackson Immuno Research, West Grove, PA), developed using enhanced chemiluminescence (ECL) (GE Healthcare Life Sciences, Pittsburgh, PA), and detected using a Nikon camera as previously described (60).

MIC2 assays. Δ*mic2e*/*mic2i* and tTA-dhfr parasites (21) were a generous gift from V. Carruthers (University of Michigan, Ann Arbor, MI). For the MIC2 knockdown experiments, Δ*mic2e*/*mic2i* tachyzoites were cultured in the presence of 2 mg/ml of ATc (Clontech, Mountain View, CA) for 2 days, and the tTA-dhfr tachyzoites were cultured in parallel. Parasites were syringe lysed from the HFF cultures, washed in high-potassium buffer, and stained with either 20 μM CellTracker CMPTX (Life Technologies, Carlsbad, CA) or 10 μM carboxyfluorescein succinimidyl ester (CFSE) (Life Technologies) in high-potassium buffer. In control experiments, we confirmed that these dyes do not have an effect on tachyzoite adhesion or motility. Nonetheless, we alternated the dyes on the parental and knockdown parasites in each experimental run to control for this possibility. A 1:1 mixture of parasites at 5×10^6 to 10×10^6/ml was perfused at 0.5 dyne/cm^2 into the microfluidic channel. For adhesion assays (Fig. 8C), the parasites were perfused for 3 min, and live images were acquired along the entire length of the channel using a 10× objective. The total number of adherent parasites in both populations was then quantified and normalized to the input ratio, as determined by flow cytometry and fluorescence microscopy. The sustained adhesion assays (Fig. 8D) were performed as described above except that a mixture of dyed tTA-dhfr and ATc-treated Δ*mic2e*/*mic2i* tachyzoites was used.

Statistical analysis. Prism Software was used to perform all statistical analyses. A one-way analysis of variance (ANOVA) with a Tukey comparison of all means was used to compare multiple means in Fig. 1B. Student's two-tailed *t* test with Welch's correction was used for pairwise comparisons in Fig. 2B, 7B, 8C, and 8D and in Fig. S3 in the supplemental material.

SUPPLEMENTAL MATERIAL

Supplemental material for this article may be found at http://mbio.asm.org/lookup/suppl/doi:10.1128/mBio.01111-13/-/DCSupplemental.

Figure S1, TIF file, 1 MB.
Figure S2, TIF file, 0.5 MB.
Figure S3, TIF file, 0.4 MB.
Video S1, MOV file, 0.5 MB.
Video S2, MOV file, 0.5 MB.
Video S3, MOV file, 0.1 MB.
Video S4, MOV file, 0.1 MB.
Video S5, MOV file, 0.1 MB.
Video S6, MOV file, 0.2 MB.

ACKNOWLEDGMENTS

We thank all the members of the Morrissette, Prescher, Tenner, and Nelson labs for thoughtful discussion of the project. We also thank Michael Buchmeier for the generous use of his microscope and Peter Bradley for sharing the GRA7 antibody. Lastly, we are grateful to Vern Carruthers and My-Hang Huynh for sharing parasite strains and antibodies and for their helpful discussion of the project.

This work was supported by ACS IRG-98-279-07 (M.B.L.), AHA Scientist Development Grant 10SDG3140025 (M.B.L.), Hellman Fellows Award (M.B.L.), NIH Immunology Training Grant T32 AI60573 (K.H.), NIH NIDCR DP2DE023319 (W.F.L.), NIH T32 Systems Biology of Development Training Grant (F.Y.M.), and set-up funds from the UC Irvine School of Biological Sciences (M.B.L.).

REFERENCES

1. **Montoya JG, Liesenfeld O.** 2004. Toxoplasmosis. Lancet **363:**1965–1976. http://dx.doi.org/10.1016/S0140-6736(04)16412-X.
2. **Dubey JP, Speer CA, Shen SK, Kwok OC, Blixt JA.** 1997. Oocyst-induced murine toxoplasmosis: life cycle, pathogenicity, and stage conversion in mice fed *Toxoplasma gondii* oocysts. J. Parasitol. **83:**870–882. http://dx.doi.org/10.2307/3284282.
3. **Lambert H, Barragan A.** 2010. Modelling parasite dissemination: host cell subversion and immune evasion by *Toxoplasma gondii*. Cell. Microbiol. **12:**292–300. http://dx.doi.org/10.1111/j.1462-5822.2009.01417.x.
4. **Dubey JP.** 1997. Tissue cyst tropism in *Toxoplasma gondii*: a comparison of tissue cyst formation in organs of cats, and rodents fed oocysts. Parasitology **115:**15–20. http://dx.doi.org/10.1017/S0031182097008949.
5. **Courret N, Darche S, Sonigo P, Milon G, Buzoni-Gâtel D, Tardieux I.** 2006. CD11c$^-$ and CD11b-expressing mouse leukocytes transport single *Toxoplasma gondii* tachyzoites to the brain. Blood **107:**309–316. http://dx.doi.org/10.1182/blood-2005-02-0666.
6. **Lambert H, Hitziger N, Dellacasa I, Svensson M, Barragan A.** 2006. Induction of dendritic cell migration upon *Toxoplasma gondii* infection potentiates parasite dissemination. Cell. Microbiol. **8:**1611–1623. http://dx.doi.org/10.1111/j.1462-5822.2006.00735.x.
7. **Lambert H, Dellacasa-Lindberg I, Barragan A.** 2011. Migratory responses of leukocytes infected with *Toxoplasma gondii*. Microbes Infect. **13:**96–102. http://dx.doi.org/10.1016/j.micinf.2010.10.002.
8. **Harker KS, Ueno N, Wang T, Bonhomme C, Liu W, Lodoen MB.** 2013. *Toxoplasma gondii* modulates the dynamics of human monocyte adhesion to vascular endothelium under fluidic shear stress. J. Leukoc. Biol. **93:**789–800. http://dx.doi.org/10.1189/jlb.1012517.
9. **Ueno N, Harker KS, Clarke EV, McWhorter FY, Liu WF, Tenner AJ, Lodoen MB.** 2014. Real-time imaging of Toxoplasma-infected human monocytes under fluidic shear stress reveals rapid translocation of intracellular parasites across endothelial barriers. Cell. Microbiol. **16**(4):580–595. http://dx.doi.org/10.1111/cmi.12239.
10. **Silveira C, Vallochi AL, Rodrigues da Silva U, Muccioli C, Holland GN, Nussenblatt RB, Belfort R, Rizzo LV.** 2011. *Toxoplasma gondii* in the peripheral blood of patients with acute and chronic toxoplasmosis. Br. J. Ophthalmol. **95:**396–400. http://dx.doi.org/10.1136/bjo.2008.148205.
11. **Barragan A, Sibley LD.** 2002. Transepithelial migration of *Toxoplasma gondii* is linked to parasite motility and virulence. J. Exp. Med. **195:**1625–1633. http://dx.doi.org/10.1084/jem.20020258.
12. **Furtado JM, Bharadwaj AS, Chipps TJ, Pan Y, Ashander LM, Smith JR.** 2012. *Toxoplasma gondii* tachyzoites cross retinal endothelium assisted by intercellular adhesion molecule-1 in vitro. Immunol. Cell Biol. **90:**912–915.
13. **Sibley LD.** 2010. How apicomplexan parasites move in and out of cells. Curr. Opin. Biotechnol. **21:**592–598. http://dx.doi.org/10.1016/j.copbio.2010.05.009.
14. **Jewett TJ, Sibley LD.** 2003. Aldolase forms a bridge between cell surface adhesins and the actin cytoskeleton in apicomplexan parasites. Mol. Cell **11:**885–894. http://dx.doi.org/10.1016/S1097-2765(03)00113-8.
15. **Dobrowolski JM, Sibley LD.** 1996. Toxoplasma invasion of mammalian cells is powered by the actin cytoskeleton of the parasite. Cell **84:**933–939. http://dx.doi.org/10.1016/S0092-8674(00)81071-5.
16. **Dobrowolski JM, Niesman IR, Sibley LD.** 1997. Actin in the parasite *Toxoplasma gondii* is encoded by a single copy gene, ACT1 and exists primarily in a globular form. Cell Motil. Cytoskeleton **37:**253–262. http://dx.doi.org/10.1002/(SICI)1097-0169(1997)37:3<253::AID-CM7>3.0.CO;2-7.
17. **Håkansson S, Morisaki H, Heuser J, Sibley LD.** 1999. Time-lapse video microscopy of gliding motility in *Toxoplasma gondii* reveals a novel, biphasic mechanism of cell locomotion. Mol. Biol. Cell **10:**3539–3547. http://dx.doi.org/10.1091/mbc.10.11.3539.
18. **Frixione E, Mondragón R, Meza I.** 1996. Kinematic analysis of *Toxoplasma gondii* motility. Cell Motil. Cytoskeleton **34:**152–163. http://dx.doi.org/10.1002/(SICI)1097-0169(1996)34:2<152::AID-CM6>3.3.CO;2-5.
19. **Ménard R.** 2001. Gliding motility and cell invasion by Apicomplexa: insights from the Plasmodium sporozoite. Cell. Microbiol. **3:**63–73. http://dx.doi.org/10.1046/j.1462-5822.2001.00097.x.
20. **Wetzel DM, Schmidt J, Kuhlenschmidt MS, Dubey JP, Sibley LD.** 2005. Gliding motility leads to active cellular invasion by Cryptosporidium parvum sporozoites. Infect. Immun. **73:**5379–5387. http://dx.doi.org/10.1128/IAI.73.9.5379-5387.2005.
21. **Huynh MH, Carruthers VB.** 2006. Toxoplasma MIC2 is a major determinant of invasion and virulence. PLoS Pathog. **2:**e84. http://dx.doi.org/10.1371/journal.ppat.0020084.
22. **Wetzel DM, Håkansson S, Hu K, Roos D, Sibley LD.** 2003. Actin

filament polymerization regulates gliding motility by apicomplexan parasites. Mol. Biol. Cell **14:**396–406. http://dx.doi.org/10.1091/mbc.E02-08-0458.
23. **Papaioannou TG, Stefanadis C.** 2005. Vascular wall shear stress: basic principles and methods. Hellenic J. Cardiol. **46:**9–15.
24. **Alon R, Feigelson SW, Manevich E, Rose DM, Schmitz J, Overby DR, Winter E, Grabovsky V, Shinder V, Matthews BD, Sokolovsky-Eisenberg M, Ingber DE, Benoit M, Ginsberg MH.** 2005. $\alpha_4\beta_1$-dependent adhesion strengthening under mechanical strain is regulated by paxillin association with the α_4-cytoplasmic domain. J. Cell Biol. **171:**1073–1084. http://dx.doi.org/10.1083/jcb.200503155.
25. **Taubert A, Krüll M, Zahner H, Hermosilla C.** 2006. *Toxoplasma gondii* and *Neospora caninum* infections of bovine endothelial cells induce endothelial adhesion molecule gene transcription and subsequent PMN adhesion. Vet. Immunol. Immunopathol. **112:**272–283. http://dx.doi.org/10.1016/j.vetimm.2006.03.017.
26. **Fischer HG, Stachelhaus S, Sahm M, Meyer HE, Reichmann G.** 1998. GRA7, an excretory 29 kDa *Toxoplasma gondii* dense granule antigen released by infected host cells. Mol. Biochem. Parasitol. **91:**251–262. http://dx.doi.org/10.1016/S0166-6851(97)00227-2.
27. **Wan KL, Carruthers VB, Sibley LD, Ajioka JW.** 1997. Molecular characterisation of an expressed sequence tag locus of *Toxoplasma gondii* encoding the micronemal protein MIC2. Mol. Biochem. Parasitol. **84:**203–214. http://dx.doi.org/10.1016/S0166-6851(96)02796-X.
28. **Carruthers VB, Sherman GD, Sibley LD.** 2000. The toxoplasma adhesive protein MIC2 is proteolytically processed at multiple sites by two parasite-derived proteases. J. Biol. Chem. **275:**14346–14353. http://dx.doi.org/10.1074/jbc.275.19.14346.
29. **Huynh MH, Rabenau KE, Harper JM, Beatty WL, Sibley LD, Carruthers VB.** 2003. Rapid invasion of host cells by Toxoplasma requires secretion of the MIC2-M2AP adhesive protein complex. EMBO J. **22:**2082–2090. http://dx.doi.org/10.1093/emboj/cdg217.
30. **Barragan A, Brossier F, Sibley LD.** 2005. Transepithelial migration of *Toxoplasma gondii* involves an interaction of intercellular adhesion molecule 1 (ICAM-1) with the parasite adhesin MIC2. Cell. Microbiol. **7:**561–568. http://dx.doi.org/10.1111/j.1462-5822.2005.00486.x.
31. **Leung JM, Rould MA, Konradt C, Hunter CA, Ward GE.** 2014. Disruption of TgPHIL1 alters specific parameters of *Toxoplasma gondii* motility measured in a quantitative, three-dimensional live motility assay. PLoS One **9:**e85763. http://dx.doi.org/10.1371/journal.pone.0085763.
32. **Ley K, Laudanna C, Cybulsky MI, Nourshargh S.** 2007. Getting to the site of inflammation: the leukocyte adhesion cascade updated. Nat. Rev. Immunol. **7:**678–689. http://dx.doi.org/10.1038/nri2156.
33. **Hegge S, Münter S, Steinbüchel M, Heiss K, Engel U, Matuschewski K, Frischknecht F.** 2010. Multistep adhesion of Plasmodium sporozoites. FASEB J. **24:**2222–2234. http://dx.doi.org/10.1096/fj.09-148700.
34. **Moriarty TJ, Shi M, Lin YP, Ebady R, Zhou H, Odisho T, Hardy PO, Salman-Dilgimen A, Wu J, Weening EH, Skare JT, Kubes P, Leong J, Chaconas G.** 2012. Vascular binding of a pathogen under shear force through mechanistically distinct sequential interactions with host macromolecules. Mol. Microbiol. **86:**1116–1131. http://dx.doi.org/10.1111/mmi.12045.
35. **Moriarty TJ, Norman MU, Colarusso P, Bankhead T, Kubes P, Chaconas G.** 2008. Real-time high resolution 3D imaging of the Lyme disease spirochete adhering to and escaping from the vasculature of a living host. PLoS Pathog. **4:**e1000090. http://dx.doi.org/10.1371/journal.ppat.1000090.
36. **Tardieux I, Ménard R.** 2008. Migration of Apicomplexa across biological barriers: the Toxoplasma and Plasmodium rides. Traffic **9:**627–635. http://dx.doi.org/10.1111/j.1600-0854.2008.00703.x.
37. **Carruthers VB, Sibley LD.** 1999. Mobilization of intracellular calcium stimulates microneme discharge in *Toxoplasma gondii*. Mol. Microbiol. **31:**421–428. http://dx.doi.org/10.1046/j.1365-2958.1999.01174.x.
38. **Wetzel DM, Chen LA, Ruiz FA, Moreno SN, Sibley LD.** 2004. Calcium-mediated protein secretion potentiates motility in *Toxoplasma gondii*. J. Cell Sci. **117:**5739–5748. http://dx.doi.org/10.1242/jcs.01495.
39. **Fruth IA, Arrizabalaga G.** 2007. *Toxoplasma gondii*: Induction of egress by the potassium ionophore nigericin. Int. J. Parasitol. **37:**1559–1567. http://dx.doi.org/10.1016/j.ijpara.2007.05.010.
40. **Carruthers VB, Håkansson S, Giddings OK, Sibley LD.** 2000. *Toxoplasma gondii* uses sulfated proteoglycans for substrate and host cell attachment. Infect. Immun. **68:**4005–4011. http://dx.doi.org/10.1128/IAI.68.7.4005-4011.2000.
41. **Soldati D, Dubremetz JF, Lebrun M.** 2001. Microneme proteins: structural and functional requirements to promote adhesion and invasion by the apicomplexan parasite *Toxoplasma gondii*. Int. J. Parasitol. **31:**1293–1302. http://dx.doi.org/10.1016/S0020-7519(01)00257-0.
42. **Friedrich N, Santos JM, Liu Y, Palma AS, Leon E, Saouros S, Kiso M, Blackman MJ, Matthews S, Feizi T, Soldati-Favre D.** 2010. Members of a novel protein family containing microneme adhesive repeat domains act as sialic acid-binding lectins during host cell invasion by apicomplexan parasites. J. Biol. Chem. **285:**2064–2076. http://dx.doi.org/10.1074/jbc.M109.060988.
43. **Blumenschein TM, Friedrich N, Childs RA, Saouros S, Carpenter EP, Campanero-Rhodes MA, Simpson P, Chai W, Koutroukides T, Blackman MJ, Feizi T, Soldati-Favre D, Matthews S.** 2007. Atomic resolution insight into host cell recognition by *Toxoplasma gondii*. EMBO J. **26:**2808–2820. http://dx.doi.org/10.1038/sj.emboj.7601704.
44. **Garcia-Réguet N, Lebrun M, Fourmaux MN, Mercereau-Puijalon O, Mann T, Beckers CJ, Samyn B, Van Beeumen J, Bout D, Dubremetz JF.** 2000. The microneme protein MIC3 of *Toxoplasma gondii* is a secretory adhesin that binds to both the surface of the host cells and the surface of the parasite. Cell. Microbiol. **2:**353–364. http://dx.doi.org/10.1046/j.1462-5822.2000.00064.x.
45. **Cérède O, Dubremetz JF, Soête M, Deslée D, Vial H, Bout D, Lebrun M.** 2005. Synergistic role of micronemal proteins in *Toxoplasma gondii* virulence. J. Exp. Med. **201:**453–463. http://dx.doi.org/10.1084/jem.20041672.
46. **Jacquet A, Coulon L, De Nève J, Daminet V, Haumont M, Garcia L, Bollen A, Jurado M, Biemans R.** 2001. The surface antigen SAG3 mediates the attachment of *Toxoplasma gondii* to cell-surface proteoglycans. Mol. Biochem. Parasitol. **116:**35–44. http://dx.doi.org/10.1016/S0166-6851(01)00297-3.
47. **Dzierszinski F, Mortuaire M, Cesbron-Delauw MF, Tomavo S.** 2000. Targeted disruption of the glycosylphosphatidylinositol-anchored surface antigen SAG3 gene in *Toxoplasma gondii* decreases host cell adhesion and drastically reduces virulence in mice. Mol. Microbiol. **37:**574–582.
48. **Aird WC.** 2007. Phenotypic heterogeneity of the endothelium: I. Structure, function, and mechanisms. Circ. Res. **100:**158–173. http://dx.doi.org/10.1161/01.RES.0000255691.76142.4a.
49. **Dupont CD, Christian DA, Hunter CA.** 2012. Immune response and immunopathology during toxoplasmosis. Semin. Immunopathol. **34:**793–813. http://dx.doi.org/10.1007/s00281-012-0339-3.
50. **Lachenmaier SM, Deli MA, Meissner M, Liesenfeld O.** 2011. Intracellular transport of *Toxoplasma gondii* through the blood-brain barrier. J. Neuroimmunol. **232:**119–130. http://dx.doi.org/10.1016/j.jneuroim.2010.10.029.
51. **Nagineni CN, Detrick B, Hooks JJ.** 2000. *Toxoplasma gondii* infection induces gene expression and secretion of interleukin 1 (IL-1), IL-6, granulocyte-macrophage colony-stimulating factor, and intercellular adhesion molecule 1 by human retinal pigment epithelial cells. Infect. Immun. **68:**407–410. http://dx.doi.org/10.1128/IAI.68.1.407-410.2000.
52. **Gamble JR, Harlan JM, Klebanoff SJ, Vadas MA.** 1985. Stimulation of the adherence of neutrophils to umbilical vein endothelium by human recombinant tumor necrosis factor. Proc. Natl. Acad. Sci. U. S. A. **82:**8667–8671. http://dx.doi.org/10.1073/pnas.82.24.8667.
53. **Schleimer RP, Rutledge BK.** 1986. Cultured human vascular endothelial cells acquire adhesiveness for neutrophils after stimulation with interleukin 1, endotoxin, and tumor-promoting phorbol diesters. J. Immunol. **136:**649–654.
54. **Dewi BE, Takasaki T, Kurane I.** 2004. *In vitro* assessment of human endothelial cell permeability: effects of inflammatory cytokines and dengue virus infection. J. Virol. Methods **121:**171–180. http://dx.doi.org/10.1016/j.jviromet.2004.06.013.
55. **Morgado P, Ong YC, Boothroyd JC, Lodoen MB.** 2011. *Toxoplasma gondii* induces B7-2 expression through activation of JNK signal transduction. Infect. Immun. **79:**4401–4412. http://dx.doi.org/10.1128/IAI.05562-11.
56. **Endo T, Tokuda H, Yagita K, Koyama T.** 1987. Effects of extracellular potassium on acid release and motility initiation in *Toxoplasma gondii*. J. Protozool. **34:**291–295. http://dx.doi.org/10.1111/j.1550-7408.1987.tb03177.x.
57. **Kane RS, Takayama S, Ostuni E, Ingber DE, Whitesides GM.** 1999. Patterning proteins and cells using soft lithography. Biomaterials **20:**2363–2376. http://dx.doi.org/10.1016/S0142-9612(99)00165-9.
58. **Dunn JD, Ravindran S, Kim SK, Boothroyd JC.** 2008. The *Toxoplasma*

gondii dense granule protein GRA7 is phosphorylated upon invasion and forms an unexpected association with the rhoptry proteins ROP2 and ROP4. Infect. Immun. **76:**5853–5861. http://dx.doi.org/10.1128/IAI.01667-07.

59. **Lodoen MB, Gerke C, Boothroyd JC.** 2010. A highly sensitive FRET-based approach reveals secretion of the actin-binding protein toxofilin during *Toxoplasma gondii* infection. Cell. Microbiol. **12:**55–66. http://dx.doi.org/10.1111/j.1462-5822.2009.01378.x.
60. **Khoury MK, Parker I, Aswad DW.** 2010. Acquisition of chemiluminescent signals from immunoblots with a digital single-lens reflex camera. Anal. Biochem. **397:**129–131. http://dx.doi.org/10.1016/j.ab.2009.09.041.